Uncovering protein conformational dynamics within two-component viral biomolecular condensates

Alice Colyer[1], Julia Acker[2], Alexander Borodavka[2]*, Antonio N. Calabrese[1]*

[1] **Astbury Centre for Structural Molecular Biology**, School of Molecular and Cellular Biology, Faculty of Biological Sciences, University of Leeds, LS2 9JT, Leeds, United Kingdom

[2] **Department of Chemical Engineering and Biotechnology,** University of Cambridge, CB2 1QW, Cambridge, United Kingdom

Correspondence to Alexander Borodavka: ab2677@cam.ac.uk (A. Borodavka) ***and Antonio N. Calabrese*:** a.calabrese@leeds.ac.uk (A.N. Calabrese)

Running title: Protein dynamics in viral biomolecular condensates

Manuscript file is total 32 pages.

Supporting Information, 6 Pages, comprising Supporting Figures and Table.

Abstract

Biomolecular condensates selectively compartmentalise and organise biomolecules within the crowded cellular milieu and are instrumental in some disease mechanisms. Upon infection, many RNA viruses form biomolecular condensates that are often referred to as viral factories. The assembly mechanism of these viral factories remains poorly defined, but involves transient, non-stoichiometric protein/RNA interactions, making their structural characterisation challenging. Here, we sought to investigate the structural dynamics and intermolecular interactions of the key proteins responsible for condensate formation upon rotavirus infection, namely NSP2 (an RNA chaperone) and NSP5 (an intrinsically disordered protein [IDP]), using a combination of hydrogen-deuterium exchange mass spectrometry (HDX-MS), native MS and biophysical tools. Our data reveal key structural features of intrinsically disordered NSP5 that are vital for condensate assembly, and highlight inter/intra-protein interactions involved in condensate assembly. Moreover, we demonstrate that within a condensate there are altered conformational dynamics within the C-terminal region of NSP2, which has previously been shown to play a role in regulating its RNA chaperoning activity, and in the disordered regions of NSP5. We propose that altered conformational dynamics in NSP2 and NSP5 are critical for regulation of RNA annealing within a biomolecular condensate and for condensate assembly/client recruitment, respectively. Combined, our data demonstrates that the unique environment within a biomolecular condensate can tune functionally important protein conformational dynamics, which may play a crucial role in the replication of rotaviruses.

Keywords: biomolecular condensates, rotavirus, protein dynamics, native mass spectrometry, hydrogen-deuterium exchange mass spectrometry

Summary statement: Many viruses form viral factories in cells upon infection that are called biomolecular condensates. Here we have studied how the proteins NSP2 and NSP5 from rotaviruses form these structures and have found that within the unique environment of condensates protein dynamics is altered, which is important for understanding rotavirus replication mechanisms in cells.

Introduction

Biomolecular condensates are utilised within crowded cellular environments to selectively compartmentalise and organise biomolecules, facilitating a variety of cellular processes and disease mechanisms, including RNA metabolism, neurodegeneration and replication of RNA viruses (Hnisz et al. 2017; Conicella et al. 2020; Geiger et al. 2021). The formation of biomolecular condensates is often described as occurring via liquid-liquid phase separation (LLPS), which dictates that the assembly of condensates is mediated by a complex network of weak, multivalent homo- and/or heterotypic non-covalent interactions (Kilgore and Young 2022). Typically, condensate formation is driven by protein molecular scaffolds, with many protein drivers of condensate assembly possessing regions of intrinsic disorder or low sequence complexity (DiRusso et al. 2022). The 'sticker and spacer' model is frequently used to describe the sequence determinants for the formation of biomolecular condensates (Choi et al. 2020). Within IDPs / IDRs, certain residues or small groups of residues known as 'stickers' may be present that possess clustered charged, polar or hydrophobic residues (Holehouse et al. 2021). These regions subsequently form non-covalent interactions with other 'sticker' regions of the same or different proteins. 'Sticker' regions are separated by 'spacer' regions, which are often enriched in charged residues (Bremer et al. 2022). Moreover, the formation of biomolecular condensates can be driven by both disordered and folded domains within proteins. For example, folded SH3 domains involved in cellular signalling are instrumental in the formation of biomolecular condensates specifically, by interacting with proline-rich motifs (Li et al. 2012). Indeed, the protein Grb2, which has SH3 domains and Sos1, which has several proline-rich motifs coordinate the assembly of biomolecular condensates (Shin and Brangwynne 2017). Likewise, the P-granule protein PGL-1, must be folded to facilitate mRNA binding and subsequent biomolecular condensate formation (Schmidt et al. 2021).

Whether predominantly ordered or disordered, the protein scaffolds of a condensate can selectively recruit client molecules (RNA/DNA or protein) into biomolecular condensates (Banani et al. 2016). The complex, heterogeneous and transient nature of condensates makes it challenging to precisely characterise the biomolecular interactions driving condensate formation, including the interactions between scaffold molecules driving condensate assembly, and the intermolecular interactions driving client recruitment. Indeed, most of our knowledge of biomolecular condensate assembly mechanisms has been gained by studying isolated single-protein systems *in vitro* (Chatterjee et al. 2022; Ingólfsson et al. 2023), and information is more

sparse for complex multiprotein systems where heterotypic interactions between scaffold molecules are key to condensate assembly (Banani et al. 2017).

Growing evidence suggests that many viral factories (VFs) are biomolecular condensates that play pivotal roles in the replication and maturation of many RNA viruses including SARS-CoV-2, Rabies, and group A rotaviruses (RV) (Alenquer et al. 2019; Zhou et al. 2019; Perdikari et al. 2020; Geiger et al. 2021; Nevers et al. 2022; He et al. 2024). During RV infection, the key drivers of VF formation are NSP5, an 25 kDa IDP that has been suggested to form higher order oligomers (Martin et al. 2011), and the RNA chaperone NSP2 (Geiger et al. 2021), which forms a 302 kDa octameric assembly that has been studied by both X-ray crystallography and cryo-EM (Jiang et al. 2006; Hu et al. 2012)**.** Whilst there is some sequence variation (length and residues) in NSP2 and NSP5 across Group A rotaviruses, it has been shown that most variants are capable of forming VFs (Lee et al. 2024). RNA interference (RNAi) experiments have demonstrated that VF formation is unable to occur without expression of both NSP2 and NSP5 in infected cells (López et al. 2005). Similarly, expression of either NSP2 or NSP5 alone in cells does not result in the formation of structures resembling VFs, whereas co-expression of NSP2 and NSP5 in the absence of other viral proteins results in the formation of VF-like structures, providing evidence that, together, these two proteins provide the platform for subsequent VF assembly (Fabbretti et al. 1999). Thus far, it is understood that upon RV infection, NSP2 and NSP5 interact, forming biomolecular condensates at low micromolar concentrations (Geiger et al. 2021; Strauss et al. 2023) (**Figure 1**), but the interactions driving VF formation have remained elusive due to their complex and transient nature. This molecular scaffold acts to recruit viral RNA, and the key viral/host proteins needed for virus replication. Throughout the later stages of infection the condensates can change in morphology, which is thought to be as a result of NSP5 hyperphosphorylation, but the structural mechanism of client recruitment and condensate maturation is poorly understood (Eichwald et al. 2002; Sotelo et al. 2010).

Structural mass spectrometry (MS) methods, such as native MS and hydrogen-deuterium exchange MS (HDX-MS) are indispensable tools to study the architecture of dynamic systems, including IDPs, membrane proteins and large, heterogenous protein complexes (Beveridge and Calabrese 2021). Native MS can be used to inform on the stoichiometry of protein assemblies, particularly for complex stoichiometries characterised by dynamic heterogeneity, and has been used previously to study mechanisms of condensate formation (Sahin et al. 2023). HDX-MS is an extremely attractive yet underexplored tool to study the formation of biomolecular condensates, allowing analysis of protein(s) and protein complexes in solution by deuterium labelling under

physiological conditions (Masson et al. 2019). In a traditional 'bottom-up' HDX-MS experiment, protein(s) of interest are incubated with deuterium, typically on the second to hour timescale, allowing labile amides within the protein backbone to exchange for deuterium. Quantification of deuterium incorporation at the peptide level by MS can inform on the solvent accessibility of backbone amides, in addition to their involvement in intra- or intermolecular hydrogen bonding (Vinciauskaite and Masson 2023).

Herein, we deployed an *in vitro* integrative structural MS approach to study the interactions driving biomolecular condensate formation by NSP2 and NSP5 and the conformational dynamics of NSP2/NSP5. Our study reveals that the C-terminal region of NSP5 is essential for driving oligomerisation of NSP5 to form a stable decamer, and without this region, condensate formation by NSP2 and NSP5 is ablated. Additionally, we show the conformational dynamics of the C-terminal helix of NSP2 are altered within NSP2/NSP5 biomolecular condensates. NSP2 is proposed to play a role in recruiting the RNA that into VFs for packaging and dsRNA synthesis (Taraporewala and Patton 2004; Bravo et al. 2018; Bravo et al. 2020), and this C-terminal helix plays an essential role in regulating this process. Altered conformational dynamics in this region when NSP2/NSP5 form a condensate suggest a role for the condensate environment in tuning NSP2 conformational dynamics, and potentially the RNA chaperoning function of NSP2. The conformational dynamics of NSP5 are also altered within a bimolecular condensate. Together, our data are consistent with a model whereby structural transitions occur in NSP2 and NSP5 within a condensate that are key to their function, which has implications for understanding VF maturation and the initial steps underlying the formation of VFs.

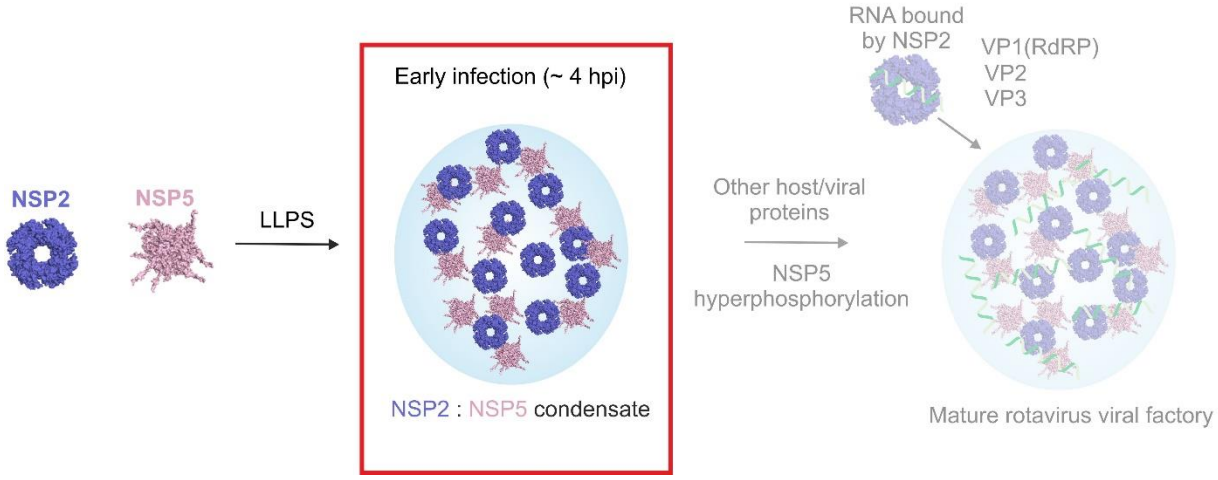

131

132 **Figure 1. Biomolecular condensate formation driven by NSP2 and NSP5.** NSP2 and NSP5
133 interact at low micromolar concentrations *in vitro* and form biomolecular condensates in RV-
134 infected cells at approximately 2-4 hours post infection (hpi) (red box). Progression of viral
135 infection is associated with RNA enrichment in VFs, likely bound by the RNA chaperone NSP2,
136 and phosphorylation of NSP5. These VFs accumulate the viral pre-genomic ssRNA, along with
137 other components of the viral replicative machinery, including the RNA Polymerase (VP1), the
138 inner capsid protein VP2, the capping enzyme (VP3), and additional capsid-forming proteins (for
139 simplicity, not shown). Here we have focused on investigating the interactions driving early
140 biomolecular condensate formation by NSP2 and NSP5 (red box).

Results

Structured regions of NSP5 are vital for condensate assembly

Whilst IDPs are typically thought of as key drivers of condensate formation, structured domains embedded within proteins that contain disordered regions also play a key role (Tibble and Gross 2023). As NSP5 is predominantly an IDP and is employed as one of the two scaffold proteins required for rotavirus VF assembly, we utilised HDX-MS to identify protected regions of NSP5, hypothesising that these would correspond to regions of (partial) structure, using a strategy we have previously described (Minshull et al. 2024). Briefly, we compared the extent of deuterium uptake between short and long deuterium-incubation time points (30s and 16 hours) (**Figure 2A**), rationalising that backbone amides which are buried, and/or involved in intra- or intermolecular hydrogen bonding will take longer to reach maximum deuterium exchange compared to solvent exposed amides and / or those that are not involved in hydrogen bonds.

A total of 21 NSP5-derived peptides were identified after digestion with pepsin, representing over 66% sequence coverage (**Supplementary Figure 1A**). We identify that in peptides derived from the 40 residues at the C-terminus of NSP5 (spanning residues 167-191 and 194-202) there appears to be protection from deuterium exchange, suggesting this C-terminal region of NSP5 is likely to possess partial structure (**Figure 2B and Supplementary Figure 1B and C**). This observation is supported by the AlphaFold2 model which depicts the C-terminal region of monomeric NSP5 to possess a structured α-helix (**Figure 2C**). In all but one of the peptides from the first 130 residues of NSP5, maximum exchange was achieved at 30 s (**Figure 2B and Supplementary Figure 1B and C**), suggesting that this region of NSP5 lacks strong inter- or intramolecular hydrogen bonding interactions. This is consistent with the structural model of monomeric NSP5 derived from AlphaFold2 (**Figure 2C**), which predicts that the N-terminus is predominantly disordered. We do observe protection from exchange in a peptide spanning residues 26-46 within the N-terminal region, which could suggest the presence of partial structure in this region of the protein. Interestingly, this region has been proposed previously to be involved in NSP2 binding (Martin et al. 2011).

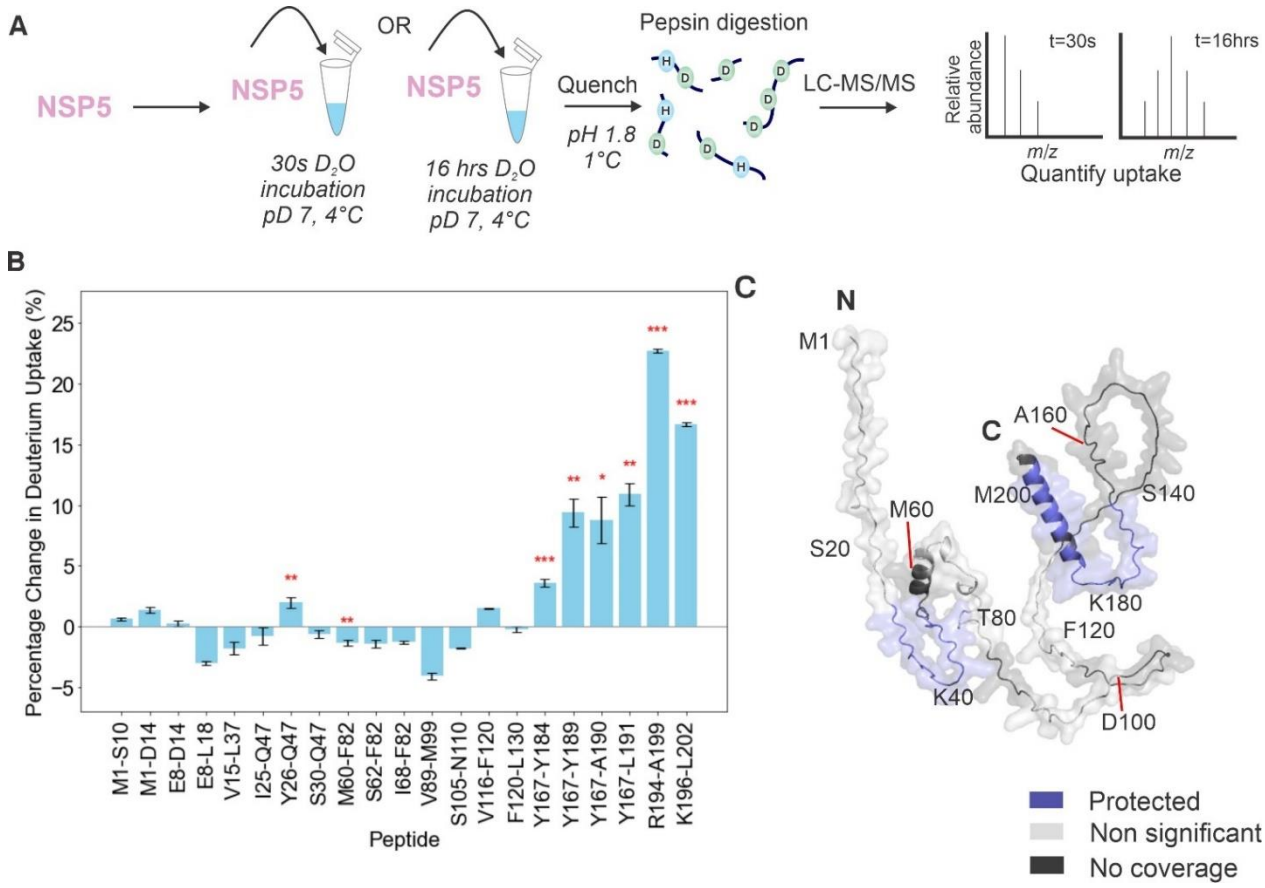

Figure 2. Identifying structured regions in the IDP NSP5 using HDX-MS. (A) Experimental schematic. NSP5 was incubated with deuterium for either 30 seconds or 16 hours before quenching of the exchange reaction by lowering the pH and temperature (see Methods). Digestion with pepsin followed by LC-MS/MS enabled the mass increase from deuterium incorporation to be quantified at the peptide level. (B) The percentage change in deuterium uptake for each peptide was calculated by dividing the difference in deuterium uptake (between 30 seconds and 16 hours for each peptide) by the maximum deuterium uptake for each peptide. The standard error was propagated to account for uncertainty with uptake measurements. A t-test was performed to identify statistically significant differences in uptake for each peptide (* = p-value <0.05, ** = p-value < 0.02, and *** = p-value <0.01) (C) AlphaFold2 model of monomeric NSP5 with protected regions (where there is a significant increase in deuterium uptake at 16 hours vs 30 seconds labelling) in blue. Regions where there was no significant increase in deuterium uptake at 16 hours are shown in light grey and regions of no coverage are shown in dark grey. For clarity, the position of every twentieth residue is labelled in the chain.

We, and others (Martin et al. 2011; Geiger et al. 2021), hypothesised that the C-terminal region of NSP5 plays a role in mediating protein oligomerisation, however the precise oligomeric state adopted by NSP5 has remained ambiguous. Therefore, we utilised native MS to interrogate the oligomeric state of NSP5 and an NSP5 variant where the C-terminal region (CTR) was removed (NSP5-ΔCTR). We chose to eliminate this folded region from NSP5, as opposed to introducing point mutations, to definitively uncover the role of the NSP5-CTR in forming higher order oligomers. Whilst this approach means we are unable to uncover specific residues which could be involved in oligomerisation, this does enable a conclusive evaluation of the role of the NSP5-CTR in oligomer formation, guided by our HDX-MS data which identified a protected C-terminus. In agreement with previous data from multi-angle light scattering (Martin et al. 2011), the native mass spectrum of NSP5 is consistent with the protein forming a stable decamer (**Figure 3A**). Strikingly, in the mass spectrum of NSP5-ΔCTR only monomeric NSP5 was detected, demonstrating that the CTR of NSP5 is essential for oligomerisation, as removal prevents the formation of higher order assemblies (**Figure 3A and B**). Given our HDX-MS data, and the AlphaFold2 structural prediction, we sought to understand the role of the folded C-terminal region in condensate formation, which revealed that removal of the NSP5-CTR abrogates condensate formation when the protein is mixed with NSP2 (**Figure 3C and 3D**). Together, these data highlight the synergistic relationship between structure, oligomerisation, and the ability of proteins to form condensates.

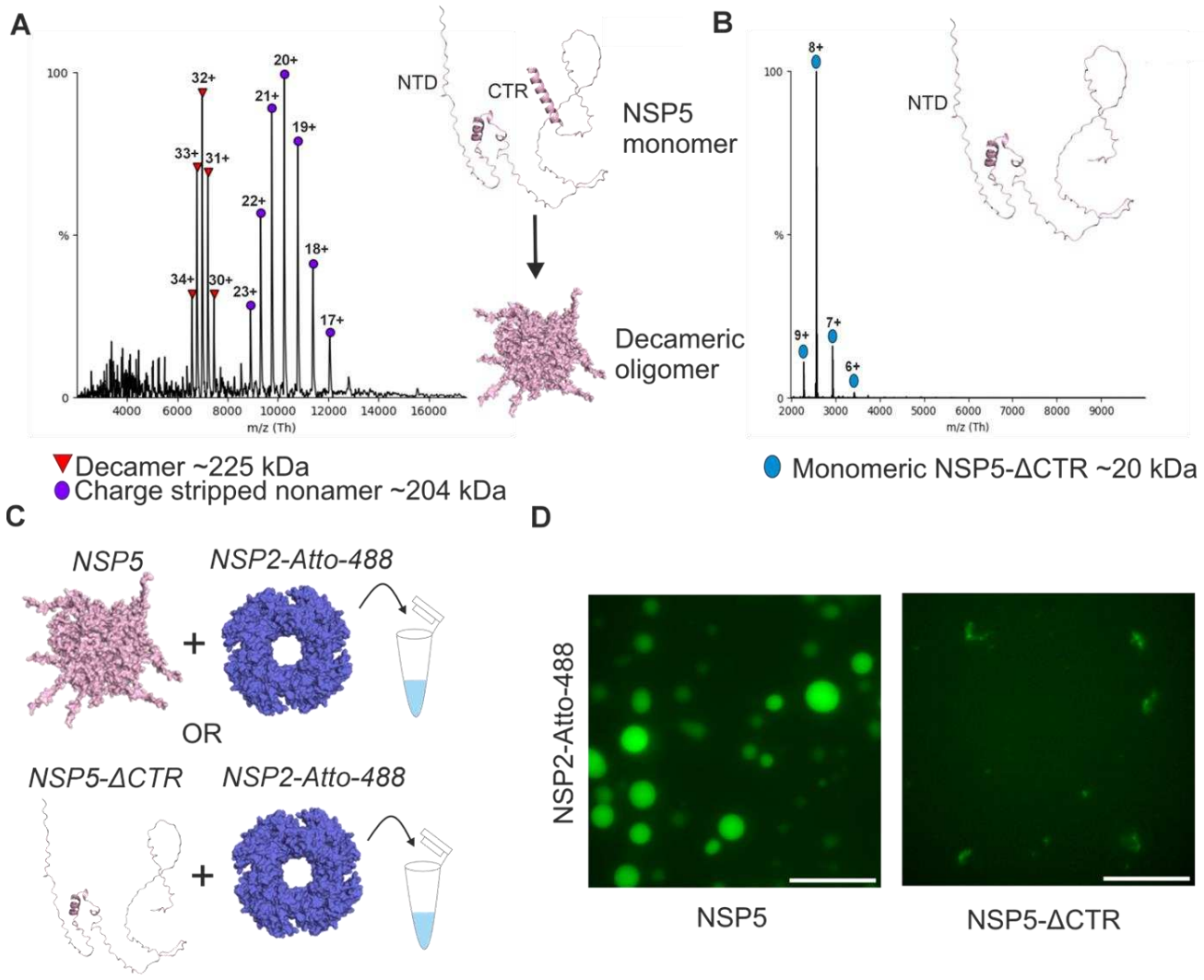

206

207 **Figure 3. The C-terminal region of NSP5 drives NSP5 oligomerisation and is essential for**
208 **biomolecular condensate formation by NSP2 and NSP5.** (A) Native mass spectrum of NSP5.
209 Red triangles represent the decameric assembly, whilst purple circles represent the charge
210 stripped nonamer formed in the gas-phase via collision induced dissociation (Belov et al. 2013).
211 (B) Native mass spectrum of NSP5-ΔCTR. Native MS experiments were performed using a
212 ThermoFisher Q-Exactive UHMR (see Methods). (C) Experimental schematic, demonstrating the
213 method used to uncover the role of the NSP5-CTR in biomolecular condensate formation driven
214 by NSP2 and NSP5. NSP2 labelled with Atto-488 was mixed with NSP5 or NSP5-ΔCTR at 15μM
215 and 30 μM respectively and immediately imaged using an ONI Nanoimager S. (D) Wide-field
216 fluorescence microscopy images of spherical biomolecular condensates formed by NSP2 and
217 NSP5 (scale bar = 10 μm, left panel). Removal of the CTR results in NSP5 that fails to form
218 biomolecular condensates when mixed with NSP2 (right panel).

Elucidating protein structural dynamics within biomolecular condensates formed by NSP2 and NSP5

The formation of biomolecular condensates relies on protein concentration, solvent conditions and inter/intra-protein hydrogen bonding. Here we sought to interrogate condensate assembly using HDX-MS, and thus first sought to establish that the labelling conditions used for the experiment will not perturb condensate formation. Fluorescence microscopy confirms that under HDX-MS buffer conditions mixtures of NSP2 and NSP5 form biomolecular condensates, that condensates dissociate under the quench conditions used in the HDX-MS experiment, and that there appears to be no aggregate formation under these conditions (**Figure 4A, Supplementary Figure 2**). The fact that condensate formation is consistent with HDX-MS buffer conditions, and reversible upon quenching confirms that NSP2/NSP5 condensates are amenable for study by HDX-MS.

HDX-MS analysis was then performed to compare the extent of protection/deprotection from exchange in NSP5 in the presence and absence or NSP2 (i.e. in dispersed versus condensed phases). Sequence coverage of NSP5 obtained post assignment was 67.5% across 15 peptides with a redundancy of 1.28 (**Supplementary Figure 3A**). Under condensate forming conditions, in the presence of NSP2, there are two protected and four deprotected NSP5 peptides (**Figure 4B**). Regions of NSP5 that become protected upon incubation with NSP2 lie within the disordered N-terminal region (residues 26-47) (**Figure 4B and C, Supplementary Figure 3B**) and in some of the proposed structured CTR of NSP5 (residues 167-191), in addition to a stretch of residues leading up to this region (**Figure 4B and C, Supplementary Figure 3B**). The regions where protection from exchange was observed may be involved in interactions that facilitate NSP5 oligomerisation that are stabilised within a condensate (**Figure 3**) or be directly participating in the intermolecular interactions with NSP2 facilitating condensate assembly. Remarkably, these two regions of protection (corresponding to N terminal protected residues 26-47 and C terminal protected residues 167-191) overlap with previous reports that have indicated a role for residues both in the N and C terminal regions of NSP5 mediating interactions with NSP2. Specifically, results from pulldown assays have suggested critical roles for residues 1-33 and 180-198 (Eichwald et al. 2004; Lee et al. 2024), suggesting that the protection from exchange observed is due to NSP2 binding. Here, by leveraging HDX-MS, we uncover relevant interactions critical for condensate formation in the context of the full-length proteins. Interestingly, we observed deprotection within the disordered N-terminus, indicating that this region is more solvent exposed/less inter/intra-protein hydrogen bonded in a condensate. This could be suggestive of

252 an allosteric perturbation in NSP5 conformational dynamics within a biomolecular condensate.
253 Such an increase in solvent exposure/reduction in intra-protein hydrogen bonding with an
254 NSP2/NSP5 condensate could be important for NSP5's function as a molecular scaffold and for
255 the recruitment of additional components into maturing biomolecular condensates during the
256 course of RV infection.

257

258

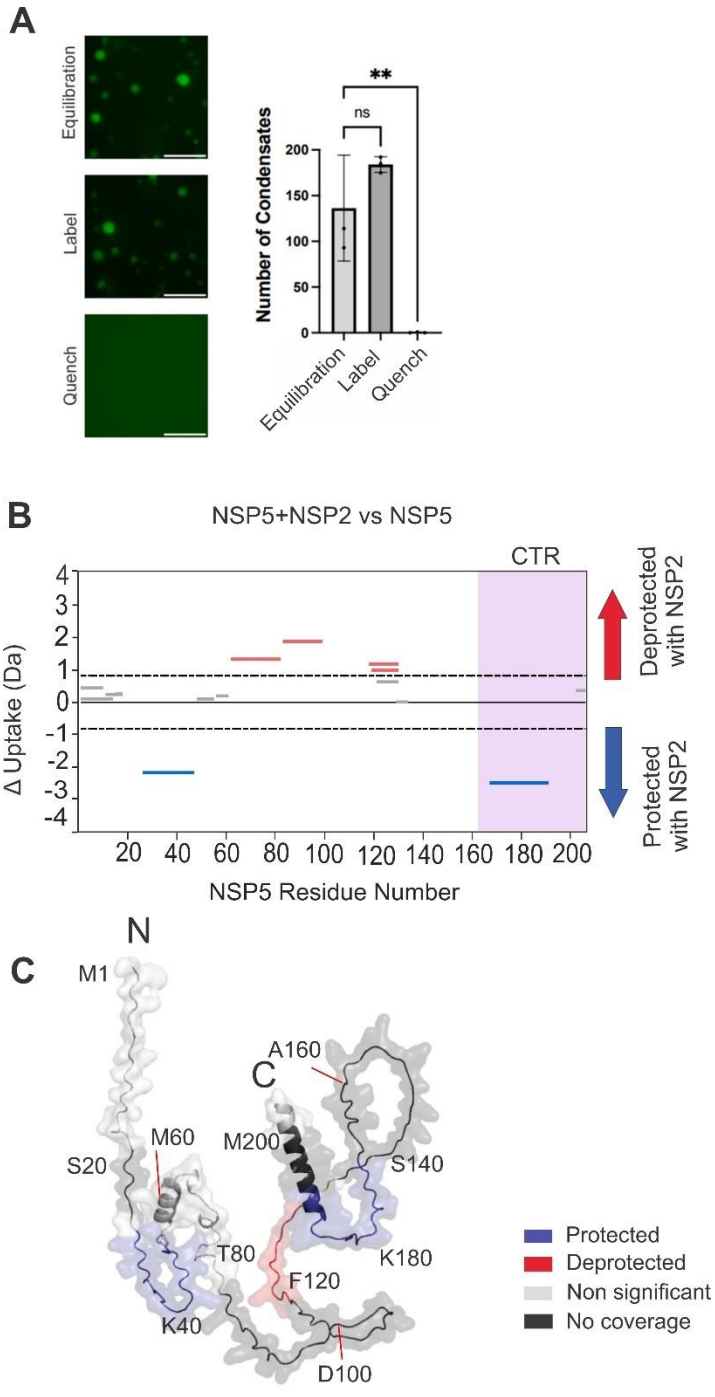

277

278 **Figure 4. HDX-MS analysis of NSP5 within a biomolecular condensate.** (A) Fluorescence
279 microscopy of NSP5 + NSP2-Atto-488 in equilibration (H_2O-containing), label (D_2O-containing),
280 and quench HDX-MS buffers. Biomolecular condensates form under deuterium labelling
281 conditions and dissociate upon quenching of the HDX reaction (scale bar = 10 µm) (left).
282 Quantification of number of condensates per field of view (right). (B) Cumulative Woods' plot

showing the summed differences in deuterium incorporation over all timepoints. Peptides from NSP5 that were significantly protected and deprotected when incubated with deuterium in the presence of NSP2 are shown in blue and red, respectively (confidence interval of 98%, see Methods). Wood's plots were produced using Deuteros (Lau et al. 2019). (C) AlphaFold2 model of monomeric NSP5 with regions of protection (blue), deprotection (red), non-significant peptides (light grey) and no coverage (dark grey), mapped on the proposed structure. For clarity, the position of every twentieth residue is labelled in the chain.

Next, we sought to identify changes in deuterium uptake in NSP2 within the condensates that form upon addition of NSP5. A total of 72.7% coverage was obtained post assignment, represented by 39 peptides (**Supplementary Figure 4A**). Interestingly, we observe a deprotected peptide (residues 245-257) in addition to a protected peptide (residues 227-244) that overlaps with the RNA binding regions on NSP2 we have previously identified (Bravo et al. 2020) (**Figure 5A**). This suggests that there may be some conformational change at or around the RNA binding sites on NSP2 within the condensate. Such changes may be important for regulating the RNA chaperone function of NSP2 (Bravo et al. 2020). Furthermore, we observe significant protection from exchange mapped to the C-terminal region of NSP2 at residues 284-305, spanning across the electropositive groove of NSP2 (**Figure 5A and B**, **Supplementary Figure 4B and C**). This is particularly interesting due to the proposed importance of the NSP2-CTR for RNA annealing, chaperone recycling (Bravo et al. 2020), VF growth and maturation (Criglar et al. 2014; Nichols et al. 2023). This observation suggests that NSP5 binding could either directly or indirectly be implicated in regulating the RNA chaperone activity of NSP2 within a condensate.

Intriguingly, upon examination of the protected NSP2 peptide spanning residues 284-305, we observed the presence of a bimodal isotopic distribution, which is unique from the typical deuterium exchange kinetics observed in most scenarios. The typical deuterium exchange process follows so-called EX2 kinetics, where a gradual incorporation of deuterium into the backbone amides of a protein is observed, because of rapid conversion (relative to the rate of deuterium exchange) between exchange incompetent and exchange competent states, and this manifests as a unimodal isotopic distribution (Hodge et al. 2020) (**Figure 5C**). In the case of NSP2, we observe that a peptide corresponding to residues 284-305 from the C-terminal helix of NSP2 uniquely appears to exhibit a bimodal isotopic distribution, even in the absence of NSP5, which is characteristic of EX1 kinetic behaviour **(Figures 5C and D)**. EX1 exchange is typical of protein regions that undergo large conformational transitions, from a closed (exchange incompetent) to an open (exchange competent) state, more slowly than the rate of deuterium exchange (Xiao 2005; Wales et al. 2013; Oganesyan et al. 2018; Hodge et al. 2020). The situation when deuterium incorporation by both EX1 and EX2 kinetic mechanisms is present is called the EXX regime (**Figure 5C**). In the presence of NSP5, the relative abundance of the ‘closed’ (exchange incompetent) form appears to increase in intensity relative to the ‘open’ (exchange competent) form. This could be because binding results in a protection from exchange, resulting in more of the ‘closed’ form being detected, or because binding is triggering a change in conformational dynamics in this region within a biomolecular condensate that favours the closed

state (**Figure 5C)**. Uncovering which scenario, or indeed if a mixture of the two scenarios is occurring is a challenge. Nevertheless, these data suggest that within a biomolecular condensate, the interaction of NSP2 with NSP5 produces an effect on the dynamic behaviour of the CTR of NSP2 **(Figure 5D)**. This change in conformational dynamics could be important for the RNA chaperoning function of NSP2, where this CTR has been shown to play a critical role (Bravo et al. 2020). In order to decouple this effect and assess if this kinetic behaviour within the NSP2 C-terminal helix is unique to biomolecular condensate formation, we performed HDX-MS of NSP2 in the presence of NSP5-ΔCTR, which we have demonstrated does not form biomolecular condensates **(Figure 3).** This revealed significant protection to residues 284-305 of NSP2, indicating that NSP5 maintains some affinity with NSP2 residues 284-305 even in the absence of biomolecular condensate formation **(Supplementary Figure 5A and B).** Strikingly, when bound to NSP5-ΔCTR, the isotopic distribution appears unimodal, characteristic of typical EX2 kinetic behaviour (i.e., rapid opening and closed reflecting protein 'breathing motions') **(Figure 5C and D).** The unimodal distribution observed here lies in between the 'closed' and 'open' forms detected when NSP2 was both alone and within a NSP2/NSP5 condensate. This suggests that in the absence of condensate formation, residues 284-305 of NSP2 are likely to exhibit an alternative conformational state in the bound state. Together, this suggests that the EX1 kinetic behaviour observed in the absence/presence of full length NSP5 (**Figure 5C**) may be a hallmark of conditions where NSP2 and NSP5 interact and form biomolecular condensates and could be suggestive of a dynamic conformational change within the C-terminal region of NSP2 that promotes RNA chaperoning.

Together, our HDX-MS data show that within a biomolecular condensate, regions of protection and deprotection are observed in both NSP2 and NSP5. Regions of deprotection in both proteins suggest that changes in conformational dynamics/hydrogen bonding arise within a biomolecular condensate. Protection in NSP2 residues 284-305 suggests that this region could be involved in stabilising condensates formed by NSP2/NSP5. However, deciphering if protection from exchange arises from either occlusion of these protein regions from solvent because of intermolecular associations or allosteric changes in dynamics/hydrogen-bonding remains a challenge and may require cross-validation with complementary methods.

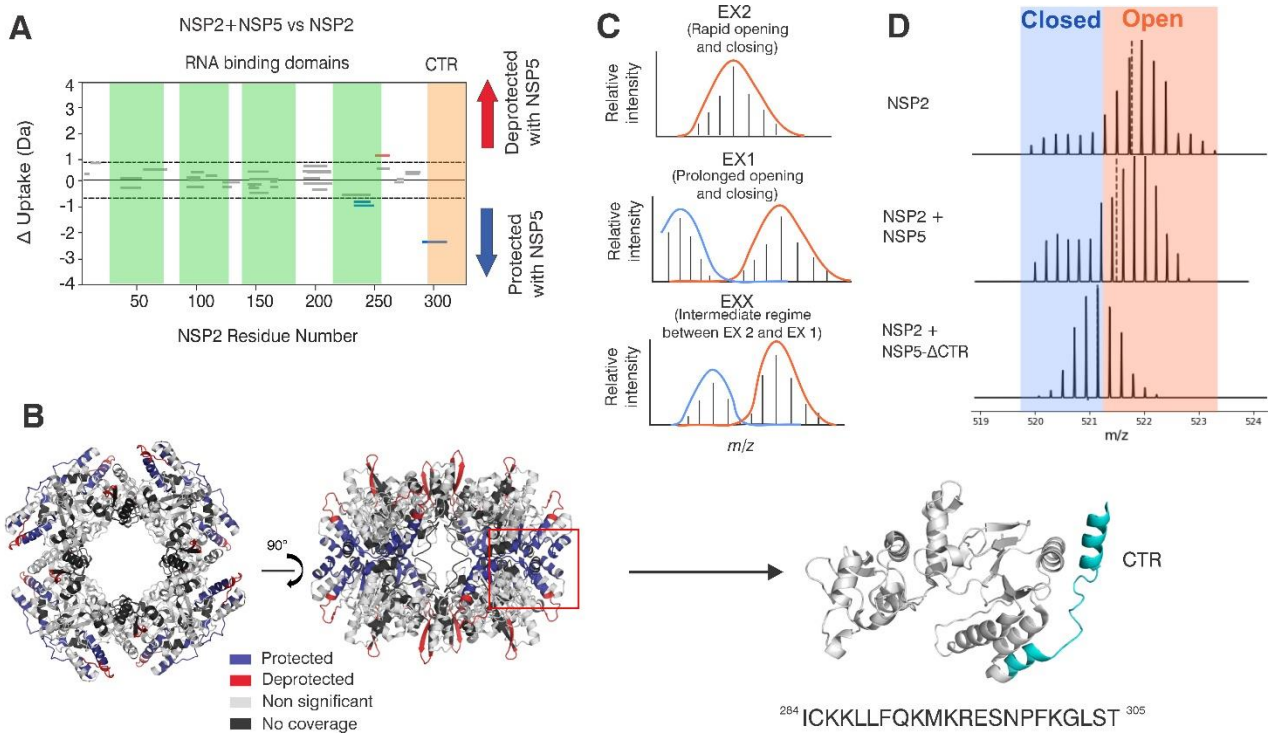

354

355 **Figure 5**. **HDX-MS analysis of NSP2 within a biomolecular condensate.** (A) Cumulative
356 Woods' plot showing the differences in deuterium incorporation over 0.5-10 min timepoints.
357 Peptides from NSP2 that were significantly protected and deprotected peptides when incubated
358 with deuterium in the presence of NSP5 are shown in blue and red, respectively (confidence
359 interval of 98%, see Methods). Produced using Deuteros (Lau et al. 2019). Green regions
360 represent proposed RNA binding regions (Bravo et al. 2020), and the C-terminal region (CTR) is
361 represented in orange. (B) NSP2 octameric structure (PDB: IL9V) with regions of protection
362 (blue), deprotection (red), non-significant peptides (light grey) and no coverage (dark grey),
363 mapped on the structure. Highlighted monomeric subunit (red box). Structure of a monomeric
364 subunit from NSP2 octamer is shown and CTR is highlighted in blue. The corresponding peptide
365 sequence (residues 284-305) is shown below the monomeric structure. (C) Schematic of
366 theoretical isotopic envelopes for EX2, EX1 and EXX kinetics detected by HDX-MS. (D)
367 Representative isotopic envelopes for a peptide spanning residues 284-305 of NSP2, for NSP2
368 alone and NSP2 + NSP5, and NSP2 + NSP5-ΔCTR after incubation with D_2O. Closed and open
369 populations represented by blue and orange boxes respectively.

Discussion

Elucidating the structure, interactions and dynamics of proteins within biomolecular condensates remains a challenging endeavour. Whilst NMR and single molecule FRET measurements have provided some insights into specific systems, these experiments are often conducted using simplistic models comprising only a single protein species (Kim et al. 2021; Galvanetto et al. 2023). This contrasts to our understanding of the mesoscale dynamics of condensates, which are relatively well characterised *in vitro* and in cell, by deployment of established methods such as FRAP (Taylor et al. 2019; Zhang and Shen 2023). Here, we show that that changes in protein structural dynamics occur in the condensate environment compared to the dispersed phase, and that these dynamic behaviours can be studied using HDX-MS.

NSP2 residues 227-244 and 284-305 could be involved in binding to residues 26-47 and 167-191 of NSP5 upon the formation of biomolecular condensates, as represented by the protected peptides in **Figures 4 and 5**. In addition, we observed deprotection spanning residues 118-130 of NSP5, suggesting weakening of the intra-protein hydrogen bonding network within NSP5. Whilst this deprotective effect is relatively small, small changes in uptake are not unexpected. The crowded nature of biomolecular condensates, which are likely to contain thousands of NSP5 molecules, would suggest any dynamic perturbations detected by HDX-MS will be an averaged measurement across the population. Given the transient and multivalent nature of interactions responsible for condensate formation (Banani et al. 2017; Darzacq and Tjian 2022), this dynamic population will be highly heterogeneous in nature, and it is therefore not surprising that changes in deuterium exchange (an ensemble averaged measurement) are small upon condensate formation. Nevertheless, the differences in deuterium exchange we have detected are statistically significant.

Intriguingly, we observe allosteric changes in dynamics in the IDP NSP5 within a condensate. Whilst allostery is more closely associated with proteins possessing defined structured regions, reports of functionally important dynamic allostery in IDPs are now emerging (Berlow et al. 2018; Bhattarai and Emerson 2020). The protection and deprotection from exchange we observed in NSP5 within a biomolecular condensate underscores the importance of NSP5 intra-protein hydrogen bonding within a condensate. We hypothesise that the deprotection we have observed (i.e. weakening of intra-protein hydrogen bonding), could help to reveal critical sequence motifs within NSP5 to facilitate its function as a molecular scaffold for client recruitment and mature viral factory assembly. Intriguingly, our data demonstrates that there is significant protection from exchange within the NSP2 C-terminal helix, which has previously been identified by X-ray

crystallography to possess both an open and closed conformation responsible for inter-octamer interactions in addition to RNA binding and nucleoside triphosphate hydrolysis activity (Hu et al. 2012). Strikingly, residue K294 of NSP2 appears to be highly dynamic in the closed- to open-state transition, experimentally confirming previous molecular dynamics simulations and reverse genetics studies of the K294E NSP2 mutant (Nichols et al. 2023). The kinetic behaviour observed in our HDX-MS experiments suggests that this region of NSP2 undergoes a specific allosteric structural change when incorporated in a condensate, or this region could be directly involved in forming 'fuzzy' interactions with NSP5 that compete with NSP2-RNA interactions (Tompa et al. 2015). We propose that a change in the structure/dynamics of this region within a biomolecular condensate may be relevant for NSP2-mediated RNA annealing and release of bound RNA from NSP2. These observations combined with previous studies, have enabled us to propose a model for NSP5/NSP2 condensate assembly, and the role of protein structural dynamics of NSP2 within a condensate (**Figure 6**).

Molecular dynamics (MD) simulations, whilst beyond the scope of this manuscript, could represent a promising future avenue to further understand and validate the protein structural dynamics we have observed here by HDX-MS within biomolecular condensates. For example, single-molecule approaches used in conjunction with MD simulations have revealed the conformational distributions and rapid structural rearrangements in a number of IDPs involved in biomolecular condensate formation on the sub-microsecond timescale (Galvanetto et al. 2023). Likewise, MD simulations of FUS (an RNA binding protein) revealed how molecular crowding influences protein dynamics within a biomolecular condensate, and how this shapes the macroscopic liquid-like properties of condensates (Mukherjee and Schäfer 2024). Furthermore, MD simulations have helped differentiate between 'fast' and 'slow' dynamics within biomolecular condensates from NMR data, demonstrating a kinetic interconversion between dilute and condensed phases, where increased intermolecular contacts under crowded environments correlate with faster dynamics (Guseva et al. 2023). Whilst we have demonstrated here that HDX-MS is able to capture peptide level resolution of the structural rearrangements within biomolecular condensates, we recognise that MD simulations could add complementary information that may aid in uncovering dynamic fluctuations in biomolecular condensates. Nevertheless, the work presented here demonstrates that with a biomolecular condensate formed by two different proteins there are changes in the dynamic behaviour of both folded and disordered regions. These changes in protein dynamics may play a critical role in facilitating condensate maturation and client recruitment, and in the case of NSP2, priming of its RNA annealing functions that are

key to viral replication. While recent advanced cryo-ET imaging can provide valuable insights into the components of viral replicative machinery and distinct structural states within biomolecular condensates (Goetz and Mahamid 2020; Tollervey et al. 2023) (De Castro et al. 2013), it cannot capture the 'fuzzy' interactions or the dynamic behaviours intrinsic to condensates formed through non-stoichiometric interactions involving multiple intrinsically disordered proteins. Our findings underscore that uncovering these protein dynamics through structural proteomics approaches is critical for understanding the mechanisms driving condensate assembly and function.

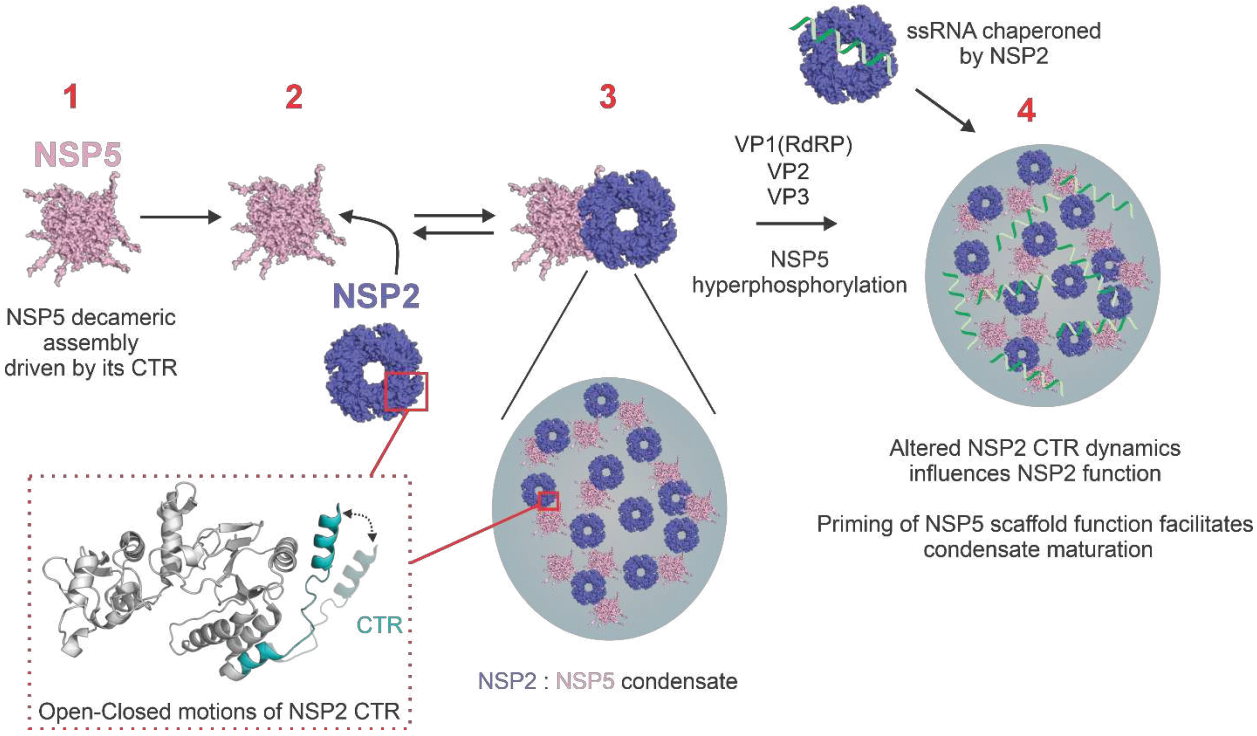

Figure 6. Proposed mechanism of biomolecular condensate formation by NSP2 and NSP5. (1) NSP5 assembles into a decameric oligomer driven by its CTR. (2) NSP5 recruits NSP2 and (3) the proteins form biomolecular condensates. Binding of NSP5 within a biomolecular condensate induces a change in conformational dynamics of the NSP2 CTR, which may contribute to RNA dissociation from NSP2 or influence inter-octamer interactions. (4) ssRNA transcripts are bound by VP1 and NSP2, and they partition into condensates along with VP2 and other capsid-forming components. Opening (measured by deprotection in HDX-MS) of the disordered regions of NSP5 facilitates client recruitment. During late stages of infection, VFs undergo maturation that correlates with NSP5 hyperphosphorylation.

Materials and Methods

Expression and purification of NSP5 and NSP2

Recombinant N-terminally Strep-tagged NSP5 RV Strain A RF and NSP5-ΔCTR were overexpressed in BL21-DE3 Gold cells prepared in-house as described by (Borodavka et al. 2017). A single colony was used to inoculate LB (100 mL) supplemented with 50 µg/ml kanamycin sulphate and incubated overnight at 37 °C shaking at 200 rpm. 10 mL of the overnight starter culture was used to inoculate LB (1 L) supplemented with 1 % glucose, 30 µM $FeCl_3$, and 50 µg/ml kanamycin sulphate. The culture was incubated at 37 °C with shaking at 200 rpm. When the culture reached an OD_{600} of 0.6, protein expression was induced by adding 1 mM IPTG and the culture was incubated overnight at 24 °C, shaking at 200 rpm. Cells were pelleted by centrifugation at 5000 xg for 20 min. The cell pellet was resuspended in lysis buffer (20 mM MOPS pH 7.1, 50 mM NaCl, 1 Complete Mini EDTA free protease inhibitor cocktail tablet per 50mL cell lysate [Roche], 1 mM DTT) and the cells lysed using a cell disruptor (Constant Flow Systems). The lysate was left at room temperature for 15 min before being supplemented with 10 µg/mL DNaseI and 10 mM $MgCl_2$. The cell lysate was left to incubate at 37°C shaking at 280 rpm for 30 min and then centrifuged at 25,000 xg for 30 min at 4°C to isolate the inclusion bodies. The inclusion bodies were resuspended in resuspension buffer (20 mM MOPS pH 7.1, 50 mM NaCl, 1 mM DTT, 0.5% Triton-X100) and centrifuged at 25,000 xg for 30 min at 4 °C. A total of 2 inclusion body washes were performed with 20 mM MOPS pH 7.1, 50 mM NaCl, 1 mM DTT, before pellets were stored at -20°C.

Inclusion bodies were solubilised in 50 mL solubilisation buffer (6 M GuHCl, 20 mM MOPS pH 7.1, 1 mM DTT) for 1 h shaking at 250 rpm at 37 °C. Insoluble material was removed by centrifugation at 3000 xg for 30 min. The supernatant was dialysed overnight against 2 L of 20 mM MOPS pH 7.1, 10 mM β-mercaptoethanol, 50 mM NaCl, 10 mM PMSF. A 5 mL StepTrap HP column (Cytiva) was equilibrated in 1 M NaCl, 20 mM MOPS pH 7.1. The supernatant was loaded onto the column and eluted over 5 column volumes of 1 M NaCl, 20 mM MOPS pH 7.1, 2 mM Desthiobiotin. Fractions were analysed by SDS PAGE and peak fractions containing NSP5 were simultaneously concentrated, and buffer exchanged into 20 mM MOPS pH 7.1 by centrifugal ultrafiltration.

Recombinant RV strain A RF C-terminally His-tagged NSP2 was overexpressed in BL21-CodonPlus (DE3)-RIL cells as per the manufacturers protocol. A single colony was used to

inoculate a starter culture of 100 mL LB supplemented with 1 % glucose and 50 µg/ml Kanamycin, and the culture was incubated overnight at 37 °C with shaking at 200 rpm. 10 mL of overnight starter culture was used to inoculate a 400 mL subculture comprising LB supplemented with 1 % glucose and 50 µg/ml Kanamycin and incubated at 37 °C shaking at 200 rpm until an OD_{600} of 0.6 was reached. Large scale 1 L cultures supplemented with 1 % glucose and 50 µg/ml Kanamycin were inoculated with 50 mL of the subculture and incubated at 37 °C with shaking at 200 rpm until they reached an OD_{600} of 0.6. Protein expression was induced with 1 mM IPTG before overnight incubation at 24 °C with shaking at 200 rpm. Cells were pelleted by centrifugation at 5000 xg for 20 min, immediately homogenised in lysis buffer (50 mM Tris-HCl pH 8.0, 300 mM NaCl, 1 Complete Mini EDTA-free protease inhibitor cocktail tablet per 50mL cell lysate [Roche]) and lysed using a cell disruptor (Constant Flow Systems) operating at 40 kpsi. 5mM β-mercaptoethanol, 10 mM $MgCl_2$ and 1mg/ml DNase was added to the lysate, and it was then incubated at room temperature for 15 min. The lysate was clarified by centrifugation (10,000 xg, 30 min, 4°C). The lysate was supplemented with 20 mM imidazole pH 8, and the protein was purified using Ni-NTA affinity chromatography using a 5 mL HisTrap FF column (Cytiva) over a linear gradient of 20 mM – 1 M imidazole for 10 CVs. Peak fractions containing NSP2 (as determined by SDS-PAGE) were combined and diluted 1:1 with 20 mM HEPES-Na pH 7.4. The protein was simultaneously concentrated, and buffer exchanged to remove residual imidazole using centrifugal ultrafiltration (Sartorius Vivaspin 50,000 MWCO). The concentrated sample was further purified by size exclusion chromatography on a HiLoad 26/600 Superdex 200pg column (Cytiva) that was pre-equilibrated with RNase-free SEC buffer (20mM HEPES, pH 7.4, 150 mM NaCl).

Fluorescence Microscopy

In vitro images were recorded using an ONI Nanoimager S equipped with a 100x 1.4 Na oil immersion objective. N-terminally tagged NSP5 and C-terminally tagged NSP2 (pre-incubated with 0.5 µM NTA-Atto-488) were mixed in equilibration buffer (1X PBS pH 7.4) or label buffer (1X PBS pH 6.6 in 100% D_2O at 4°C) to give a final concentration of 1.25 µM of each protein or in quench buffer (PBS pH 1.8 in 0.1% DDM at 1°C) to give a final concentration of 0.75µM. 4 μL of either sample was transferred to a glass cover slip and mounted on the Nanoimager. Fluorescent signal was detected by excitation of the sample with a 488 nm laser at a laser power of 2 mW. An area of 50 μm x 800 μm was recorded after 30 s, 2 m, 5 m, and 10 m incubation of the sample on the glass cover slip. ImageJ (Baggett et al. 2022) was used for automated particle counting and

image analysis, and binary images were created by using Yen's thresholding method (Jui-Cheng Yen et al. 1995).

Native Mass Spectrometry

Native MS experiments were conducted on a Q-Exactive Quadrupole Orbitrap UHMR Mass Spectrometer (Thermo Fisher) using in-house prepared gold and palladium coated nESI capillaries. Full length NSP5 was buffer exchanged into 200mM ammonium acetate pH 6.9 and NSP5-ΔCTR was buffer exchanged into 200mM ammonium acetate pH 5.5 using 7K MWCO Zeba spin desalting columns (Thermo Fisher) and diluted to a final monomeric concentration of 20 µM and 40 µM respectively. Instrument parameters were set to capillary voltage = 1.5kV, desolvation voltage = -150, resolution = 6000.

Hydrogen-Deuterium Exchange Mass Spectrometry (HDX-MS)

HDX-MS experiments were performed on an automated HDX robot (LEAP technologies, USA) coupled to an Acquity M-class LC and HDX manager (Waters Corporation, UK). For NSP2 + NSP5 and NSP2 + NSP5-ΔCTR, a total of 5 µL of protein containing solution containing NSP2 (25 µM), NSP5 / NSP5Δ-CTR (25 µM), or a mixture of both (25 µM each) was added to 95 µL of deuterated buffer (1X PBS pD 7, 95 % D_2O). Samples were incubated at 4 °C for 0, 0.5, 5 and 10 min. The exchange reaction was quenched post labelling by addition of 75 µL of quench buffer (1X PBS pH 1.8, 0.1% DDM) to 75 µL of the sample. For differential HDX-MS of NSP5 alone to identify regions of partial structure, 5µL of NSP5 at 10 µM was added to 95 µL of a deuterated buffer containing 25mM potassium phosphate, 25 mM dipotassium phosphate, 300 mM NaCl in 85.5% D_2O (pD 7) for either 30 s or 16 hr. After labelling, HDX was quenched by adding 100 µL of quench buffer containing 25 mM potassium phosphate, 25 mM dipotassium phosphate and 0.5% (w/v) DDM (pH 1.8) in 100 mL H_2O. A total of 90 µL quenched sample was passed through an immobilised pepsin column (Enzymate, Waters Corporation, UK) and the resultant peptides were trapped on a VanGuard Pre-Column (Acquity UPLC BEH C18 [17 µm, 2.1 mm x 5 mm], Waters Corporation, UK) for 3 min. Separation of peptide fragments was achieved with a C18 column (75 µm x 150 mm, Waters Corporation, UK) eluting over a linear gradient of 0-40% (v/v) acetonitrile (0.1%[v/v] formic acid) in H_2O (0.3% [v/v] formic acid) over 7 min at 40 µL min^{-1}. Peptide fragments were detected using a Synapt G2-Si mass spectrometer (Waters Corporation, UK), operated in mobility-assisted data independent analysis with dynamic range extension enabled (HDMSe).

HDX-MS analysis

Data were analysed using PLGS and DynamX software (Waters Corporation, UK). Pepsin was excluded from the analysis and restrictions for peptides in DynamX were minimum intensity = 1000, maximum sequence length = 25, minimum products per amino acid = 0.3, max ppm error = 10, file threshold = 2/3 replicates. Deuteros was used to identify statistically significant protected and deprotected peptides and to generate Woods plots (Lau et al. 2019). Statistically significant peptides were identified using an applied confidence interval of 98 % that takes into account the variance in the measured uptake values, the number of timepoint observations for the variance, the number of timepoints, and a critical value for a 98 % confidence limit for a two-tailed t-test, as outlined previously (Lau et al. 2019). A summary table of HDX-MS parameters, in accordance with community guidelines (Masson et al. 2019) can be found in **Supplementary Table 1**.

Declaration of competing interest

The authors declare no competing financial interest.

CRedIT authorship contribution statement

Alice Colyer: Writing- original draft, writing- review and editing, conceptualization, data curation, formal analysis, investigation, methodology, validation, visualisation.

Julia Acker: Writing- review and editing, conceptualization, data curation, formal analysis, investigation, methodology, validation, visualisation.

Alexander Borodavka: Writing- review and editing, conceptualization, funding acquisition, methodology, project administration, resources, software, supervision.

Antonio Calabrese: Writing- review and editing, conceptualization, funding acquisition, methodology, project administration, resources, software, supervision.

Data Availability

The HDX-MS data have been deposited to the ProteomeXchange Consortium via the PRIDE partner repository with the dataset identifier PXD058097.(Reviewer access details: Log in to the PRIDE website using the following details: Project accession: PXD058097, Token: 8NeXy0d5d4KN OR Username: reviewer_pxd058097@ebi.ac.uk, Password: GJxPVT04w1sB).

Funding

A.C. acknowledges PhD funding from the University of Leeds. J.A. acknowledges funding from the Engineering and Physical Sciences Research Council (EPSRC) doctoral training partnership (DTP) [2597129]. A.N.C. acknowledges support from a Sir Henry Dale Fellowship jointly funded by Wellcome and the Royal Society (220628/Z/20/Z). A.N.C acknowledges support of a Royal Society research grant (RGS\R2\222357). A.B. acknowledges support from a Sir Henry Dale Fellowship jointly funded by Wellcome and the Royal Society (213437/Z/18/Z), and funding from Wellcome (307249/Z/23/Z). Funding from BBSRC (BB/M012573/1) and Wellcome (208385/Z/17/Z) enabled the purchase of mass spectrometry equipment.

Acknowledgments

We thank J. Ault, R. George, S.R. Ganji and G. Wildsmith for technical support and for maintaining the Biomolecular Mass Spectrometry Facility at the University of Leeds.

References

Alenquer M, Vale-Costa S, Etibor TA, Ferreira F, Sousa AL, Amorim MJ. 2019. Influenza A virus ribonucleoproteins form liquid organelles at endoplasmic reticulum exit sites. Nat Commun. 10(1):1629. doi:10.1038/s41467-019-09549-4.

Baggett DW, Medyukhina A, Tripathi S, Shirnekhi HK, Wu H, Pounds SB, Khairy K, Kriwacki R. 2022. An Image Analysis Pipeline for Quantifying the Features of Fluorescently-Labeled Biomolecular Condensates in Cells. Front Bioinforma. 2:897238. doi:10.3389/fbinf.2022.897238.

Banani SF, Lee HO, Hyman AA, Rosen MK. 2017. Biomolecular condensates: organizers of cellular biochemistry. Nat Rev Mol Cell Biol. 18(5):285–298. doi:10.1038/nrm.2017.7.

Banani SF, Rice AM, Peeples WB, Lin Y, Jain S, Parker R, Rosen MK. 2016. Compositional Control of Phase-Separated Cellular Bodies. Cell. 166(3):651–663. doi:10.1016/j.cell.2016.06.010.

Belov ME, Damoc E, Denisov E, Compton PD, Horning S, Makarov AA, Kelleher NL. 2013. From Protein Complexes to Subunit Backbone Fragments: A Multi-stage Approach to Native Mass Spectrometry. Anal Chem. 85(23):11163–11173. doi:10.1021/ac4029328.

Berlow RB, Dyson HJ, Wright PE. 2018. Expanding the Paradigm: Intrinsically Disordered Proteins and Allosteric Regulation. J Mol Biol. 430(16):2309–2320. doi:10.1016/j.jmb.2018.04.003.

Beveridge R, Calabrese AN. 2021. Structural Proteomics Methods to Interrogate the Conformations and Dynamics of Intrinsically Disordered Proteins. Front Chem. 9:603639. doi:10.3389/fchem.2021.603639.

Bhattarai A, Emerson IA. 2020. Dynamic conformational flexibility and molecular interactions of intrinsically disordered proteins. J Biosci. 45(1):29. doi:10.1007/s12038-020-0010-4.

Borodavka A, Dykeman EC, Schrimpf W, Lamb DC. 2017. Protein-mediated RNA folding governs sequence-specific interactions between rotavirus genome segments. eLife. 6. doi:10.7554/eLife.27453.

Bravo JPK, Bartnik K, Venditti L, Gail EH, Davidovich C, Lamb DC, Tuma R, Calabrese AN, Borodavka A. 2020. Structural basis of rotavirus RNA chaperone displacement and RNA annealing. Biophysics. [accessed 2021 Mar 29]. http://biorxiv.org/lookup/doi/10.1101/2020.10.26.354233.

Bravo JPK, Borodavka A, Barth A, Calabrese AN, Mojzes P, Cockburn JJB, Lamb DC, Tuma R. 2018. Stability of local secondary structure determines selectivity of viral RNA chaperones. Nucleic Acids Res. 46(15):7924–7937. doi:10.1093/nar/gky394.

Bremer A, Farag M, Borcherds WM, Peran I, Martin EW, Pappu RV, Mittag T. 2022. Deciphering how naturally occurring sequence features impact the phase behaviours of disordered prion-like domains. Nat Chem. 14(2):196–207. doi:10.1038/s41557-021-00840-w.

643 Chatterjee S, Kan Y, Brzezinski M, Koynov K, Regy RM, Murthy AC, Burke KA, Michels JJ,
644 Mittal J, Fawzi NL, et al. 2022. Reversible Kinetic Trapping of FUS Biomolecular Condensates.
645 Adv Sci. 9(4):2104247. doi:10.1002/advs.202104247.

646 Choi J-M, Holehouse AS, Pappu RV. 2020. Physical Principles Underlying the Complex Biology
647 of Intracellular Phase Transitions. Annu Rev Biophys. 49(1):107–133. doi:10.1146/annurev-
648 biophys-121219-081629.

649 Conicella AE, Dignon GL, Zerze GH, Schmidt HB, D'Ordine AM, Kim YC, Rohatgi R, Ayala YM,
650 Mittal J, Fawzi NL. 2020. TDP-43 α-helical structure tunes liquid–liquid phase separation and
651 function. Proc Natl Acad Sci. 117(11):5883–5894. doi:10.1073/pnas.1912055117.

652 Criglar JM, Hu L, Crawford SE, Hyser JM, Broughman JR, Prasad BVV, Estes MK. 2014. A
653 Novel Form of Rotavirus NSP2 and Phosphorylation-Dependent NSP2-NSP5 Interactions Are
654 Associated with Viroplasm Assembly. J Virol. 88(2):786–798. doi:10.1128/JVI.03022-13.

655 Darzacq X, Tjian R. 2022. Weak multivalent biomolecular interactions: a strength versus
656 numbers tug of war with implications for phase partitioning. RNA N Y N. 28(1):48–51.
657 doi:10.1261/rna.079004.121.

658 De Castro IF, Volonté L, Risco C. 2013. Virus factories: biogenesis and structural design:
659 Biogenesis and architecture of virus factories. Cell Microbiol. 15(1):24–34.
660 doi:10.1111/cmi.12029.

661 DiRusso CJ, Dashtiahangar M, Gilmore TD. 2022. Scaffold proteins as dynamic integrators of
662 biological processes. J Biol Chem. 298(12):102628. doi:10.1016/j.jbc.2022.102628.

663 Eichwald C, Rodriguez JF, Burrone OR. 2004. Characterization of rotavirus NSP2/NSP5
664 interactions and the dynamics of viroplasm formation. J Gen Virol. 85(3):625–634.
665 doi:10.1099/vir.0.19611-0.

666 Eichwald C, Vascotto F, Fabbretti E, Burrone OR. 2002. Rotavirus NSP5: Mapping
667 Phosphorylation Sites and Kinase Activation and Viroplasm Localization Domains. J Virol.
668 76(7):3461–3470. doi:10.1128/JVI.76.7.3461-3470.2002.

669 Fabbretti E, Afrikanova I, Vascotto F, Burrone OR. 1999. Two non-structural rotavirus proteins,
670 NSP2 and NSP5, form viroplasm-like structures in vivo. J Gen Virol. 80(2):333–339.
671 doi:10.1099/0022-1317-80-2-333.

672 Galvanetto N, Ivanović MT, Chowdhury A, Sottini A, Nüesch MF, Nettels D, Best RB, Schuler B.
673 2023. Extreme dynamics in a biomolecular condensate. Nature. 619(7971):876–883.
674 doi:10.1038/s41586-023-06329-5.

675 Geiger F, Acker J, Papa G, Wang X, Arter WE, Saar KL, Erkamp NA, Qi R, Bravo JP, Strauss
676 S, et al. 2021. Liquid–liquid phase separation underpins the formation of replication factories in
677 rotaviruses. EMBO J. 40(21):e107711. doi:10.15252/embj.2021107711.

678 Goetz SK, Mahamid J. 2020. Visualizing Molecular Architectures of Cellular Condensates: Hints
679 of Complex Coacervation Scenarios. Dev Cell. 55(1):97–107. doi:10.1016/j.devcel.2020.09.003.

680 Guseva S, Schnapka V, Adamski W, Maurin D, Ruigrok RWH, Salvi N, Blackledge M. 2023.
681 Liquid–Liquid Phase Separation Modifies the Dynamic Properties of Intrinsically Disordered
682 Proteins. J Am Chem Soc. 145(19):10548–10563. doi:10.1021/jacs.2c13647.

683 He L, Wang Q, Wang X, Zhou F, Yang C, Li Y, Liao L, Zhu Z, Ke F, Wang Y. 2024. Liquid-liquid
684 phase separation is essential for reovirus viroplasm formation and immune evasion. Dutch RE,
685 editor. J Virol. 98(9):e01028-24. doi:10.1128/jvi.01028-24.

686 Hnisz D, Shrinivas K, Young RA, Chakraborty AK, Sharp PA. 2017. A Phase Separation Model
687 for Transcriptional Control. Cell. 169(1):13–23. doi:10.1016/j.cell.2017.02.007.

688 Hodge EA, Benhaim MA, Lee KK. 2020. Bridging protein structure, dynamics, and function
689 using hydrogen/deuterium-exchange mass spectrometry. Protein Sci. 29(4):843–855.
690 doi:10.1002/pro.3790.

691 Holehouse AS, Ginell GM, Griffith D, Böke E. 2021. Clustering of Aromatic Residues in Prion-
692 like Domains Can Tune the Formation, State, and Organization of Biomolecular Condensates:
693 Published as part of the *Biochemistry* virtual special issue “Protein Condensates.” Biochemistry.
694 60(47):3566–3581. doi:10.1021/acs.biochem.1c00465.

695 Hu L, Chow D-C, Patton JT, Palzkill T, Estes MK, Prasad BVV. 2012. Crystallographic Analysis
696 of Rotavirus NSP2-RNA Complex Reveals Specific Recognition of 5’ GG Sequence for RTPase
697 Activity. J Virol. 86(19):10547–10557. doi:10.1128/JVI.01201-12.

698 Ingólfsson HI, Rizuan A, Liu X, Mohanty P, Souza PCT, Marrink SJ, Bowers MT, Mittal J, Berry
699 J. 2023. Multiscale simulations reveal TDP-43 molecular-level interactions driving condensation.
700 Biophys J. 122(22):4370–4381. doi:10.1016/j.bpj.2023.10.016.

701 Jiang X, Jayaram H, Kumar M, Ludtke SJ, Estes MK, Prasad BVV. 2006. Cryoelectron
702 Microscopy Structures of Rotavirus NSP2-NSP5 and NSP2-RNA Complexes: Implications for
703 Genome Replication. J Virol. 80(21):10829–10835. doi:10.1128/JVI.01347-06.

704 Jui-Cheng Yen, Fu-Juay Chang, Shyang Chang. 1995. A new criterion for automatic multilevel
705 thresholding. IEEE Trans Image Process. 4(3):370–378. doi:10.1109/83.366472.

706 Kilgore HR, Young RA. 2022. Learning the chemical grammar of biomolecular condensates. Nat
707 Chem Biol. 18(12):1298–1306. doi:10.1038/s41589-022-01046-y.

708 Kim TH, Payliss BJ, Nosella ML, Lee ITW, Toyama Y, Forman-Kay JD, Kay LE. 2021.
709 Interaction hot spots for phase separation revealed by NMR studies of a CAPRIN1 condensed
710 phase. Proc Natl Acad Sci. 118(23):e2104897118. doi:10.1073/pnas.2104897118.

711 Lau AMC, Ahdash Z, Martens C, Politis A. 2019. Deuteros: software for rapid analysis and
712 visualization of data from differential hydrogen deuterium exchange-mass spectrometry.
713 Valencia A, editor. Bioinformatics. 35(17):3171–3173. doi:10.1093/bioinformatics/btz022.

714 Lee M, Cosic A, Tobler K, Aguilar C, Fraefel C, Eichwald C. 2024. Characterization of
715 viroplasm-like structures by co-expression of NSP5 and NSP2 across rotavirus species A to J. J
716 Virol. 98(9):e0097524. doi:10.1128/jvi.00975-24.

717 Li P, Banjade S, Cheng H-C, Kim S, Chen B, Guo L, Llaguno M, Hollingsworth JV, King DS,
718 Banani SF, et al. 2012. Phase transitions in the assembly of multivalent signalling proteins.
719 Nature. 483(7389):336–340. doi:10.1038/nature10879.

720 López T, Rojas M, Ayala-Bretón C, López S, Arias CF. 2005. Reduced expression of the
721 rotavirus NSP5 gene has a pleiotropic effect on virus replication. J Gen Virol. 86(6):1609–1617.
722 doi:10.1099/vir.0.80827-0.

723 Martin D, Ouldali M, Ménétrey J, Poncet D. 2011. Structural Organisation of the Rotavirus
724 Nonstructural Protein NSP5. J Mol Biol. 413(1):209–221. doi:10.1016/j.jmb.2011.08.008.

725 Masson GR, Burke JE, Ahn NG, Anand GS, Borchers C, Brier S, Bou-Assaf GM, Engen JR,
726 Englander SW, Faber J, et al. 2019. Recommendations for performing, interpreting and
727 reporting hydrogen deuterium exchange mass spectrometry (HDX-MS) experiments. Nat
728 Methods. 16(7):595–602. doi:10.1038/s41592-019-0459-y.

729 Minshull TC, Byrd EJ, Olejnik M, Calabrese AN. 2024. Hydrogen–Deuterium Exchange Mass
730 Spectrometry Reveals Mechanistic Insights into RNA Oligonucleotide-Mediated Inhibition of
731 TDP-43 Aggregation. J Am Chem Soc. 146(49):33626–33639. doi:10.1021/jacs.4c11229.

732 Mukherjee S, Schäfer LV. 2024. Heterogeneous Slowdown of Dynamics in the Condensate of
733 an Intrinsically Disordered Protein. J Phys Chem Lett. 15(45):11244–11251.
734 doi:10.1021/acs.jpclett.4c02142.

735 Nevers Q, Scrima N, Glon D, Le Bars R, Decombe A, Garnier N, Ouldali M, Lagaudrière-
736 Gesbert C, Blondel D, Albertini A, et al. 2022. Properties of rabies virus phosphoprotein and
737 nucleoprotein biocondensates formed in vitro and in cellulo. Altmeyer R, editor. PLOS Pathog.
738 18(12):e1011022. doi:10.1371/journal.ppat.1011022.

739 Nichols SL, Nilsson EM, Brown-Harding H, LaConte LEW, Acker J, Borodavka A, McDonald
740 Esstman S. 2023. Flexibility of the Rotavirus NSP2 C-Terminal Region Supports Factory
741 Formation via Liquid-Liquid Phase Separation. López S, editor. J Virol. 97(2):e00039-23.
742 doi:10.1128/jvi.00039-23.

743 Oganesyan I, Lento C, Wilson DJ. 2018. Contemporary hydrogen deuterium exchange mass
744 spectrometry. Methods San Diego Calif. 144:27–42. doi:10.1016/j.ymeth.2018.04.023.

745 Perdikari TM, Murthy AC, Ryan VH, Watters S, Naik MT, Fawzi NL. 2020. SARS-CoV-2
746 nucleocapsid protein undergoes liquid-liquid phase separation stimulated by RNA and partitions
747 into phases of human ribonucleoproteins. Biochemistry. [accessed 2023 Jul 11].
748 http://biorxiv.org/lookup/doi/10.1101/2020.06.09.141101.

749 Sahin C, Motso A, Gu X, Feyrer H, Lama D, Arndt T, Rising A, Gese GV, Hällberg BM,
750 Marklund ErikG, et al. 2023. Mass Spectrometry of RNA-Binding Proteins during Liquid–Liquid
751 Phase Separation Reveals Distinct Assembly Mechanisms and Droplet Architectures. J Am
752 Chem Soc. 145(19):10659–10668. doi:10.1021/jacs.3c00932.

753 Schmidt H, Putnam A, Rasoloson D, Seydoux G. 2021. Protein-based condensation
754 mechanisms drive the assembly of RNA-rich P granules. eLife. 10:e63698.
755 doi:10.7554/eLife.63698.

Sotelo PH, Schümann M, Krause E, Chnaiderman J. 2010. Analysis of rotavirus non-structural protein NSP5 by mass spectrometry reveals a complex phosphorylation pattern. Virus Res. 149(1):104–108. doi:10.1016/j.virusres.2009.12.006.

Strauss S, Acker J, Papa G, Desirò D, Schueder F, Borodavka A, Jungmann R. 2023. Principles of RNA recruitment to viral ribonucleoprotein condensates in a segmented dsRNA virus. eLife. 12:e68670. doi:10.7554/eLife.68670.

Taraporewala ZF, Patton JT. 2004. Nonstructural proteins involved in genome packaging and replication of rotaviruses and other members of the Reoviridae. Virus Res. 101(1):57–66. doi:10.1016/j.virusres.2003.12.006.

Taylor NO, Wei M-T, Stone HA, Brangwynne CP. 2019. Quantifying Dynamics in Phase-Separated Condensates Using Fluorescence Recovery after Photobleaching. Biophys J. 117(7):1285–1300. doi:10.1016/j.bpj.2019.08.030.

Tibble RW, Gross JD. 2023. A call to order: Examining structured domains in biomolecular condensates. J Magn Reson. 346:107318. doi:10.1016/j.jmr.2022.107318.

Tollervey F, Zhang X, Bose M, Sachweh J, Woodruff JB, Franzmann TM, Mahamid J. 2023. Cryo-Electron Tomography of Reconstituted Biomolecular Condensates. In: Zhou H-X, Spille J-H, Banerjee PR, editors. Phase-Separated Biomolecular Condensates. Vol. 2563. New York, NY: Springer US. (Methods in Molecular Biology). p. 297–324. [accessed 2024 Nov 6]. https://link.springer.com/10.1007/978-1-0716-2663-4_15.

Tompa P, Schad E, Tantos A, Kalmar L. 2015. Intrinsically disordered proteins: emerging interaction specialists. Curr Opin Struct Biol. 35:49–59. doi:10.1016/j.sbi.2015.08.009.

Vinciauskaite V, Masson GR. 2023. Fundamentals of HDX-MS. Britt H, Beveridge R, Calabrese A, editors. Essays Biochem. 67(2):301–314. doi:10.1042/EBC20220111.

Wales TE, Eggertson MJ, Engen JR. 2013. Considerations in the analysis of hydrogen exchange mass spectrometry data. Methods Mol Biol Clifton NJ. 1007:263–288. doi:10.1007/978-1-62703-392-3_11.

Xiao H. 2005. Mapping protein energy landscapes with amide hydrogen exchange and mass spectrometry: I. A generalized model for a two-state protein and comparison with experiment. Protein Sci. 14(2):543–557. doi:10.1110/ps.041001705.

Zhang Y, Shen L. 2023. An in vitro Assay to Probe the Formation of Biomolecular Condensates. Bio-Protoc. 13(17):e4813. doi:10.21769/BioProtoc.4813.

Zhou Y, Su JM, Samuel CE, Ma D. 2019. Measles Virus Forms Inclusion Bodies with Properties of Liquid Organelles. Dutch RE, editor. J Virol. 93(21):e00948-19, /jvi/93/21/JVI.00948-19.atom. doi:10.1128/JVI.00948-19.